AIAA AVIATION Forum
17-21 June 2019, Dallas, Texas
AIAA Aviation 2019 Forum

10.2514/6.2019-3576

Development of A Certification Module for Early Aircraft Design

Jiacheng Xie*, Simon Briceno†, and Dimitri N. Mavris‡
Aerospace Systems Design Laboratory, School of Aerospace Engineering
Georgia Institute of Technology, Atlanta, Georgia, 30332

Imon Chakraborty§
Department of Aerospace Engineering
Auburn University, Auburn, Alabama, 36849

The airworthiness certification process of civil transportation aircraft is expensive, time-consuming, and subject to uncertainty. To reduce the cost and time spent on the certification process, this paper proposes an approach to incorporate certification considerations into early design stages using virtual certification techniques. As a proof of concept, this paper focuses on flight performance certification requirements and developed a certification analysis module for aircraft conceptual and early preliminary design based on FAR-25 Subpart B. The module transforms the regulations from textual documents to quantitative constraint functions and ensures the certification constraint check of the design through physics-based analysis. To validate the module, a Small Single-aisle Aircraft testing model is developed and virtually certified by the module. The certification analysis result of the testing model is benchmarked with public domain data.

I. Nomenclature

α	=	angle of attack
β	=	sideslip angle
θ	=	pitch attitude
γ	=	flight path angle
ϕ	=	bank attitude
ψ	=	yaw attitude
δ_a	=	aileron deflection
δ_e	=	elevator defection
δ_r	=	rudder deflection
b	=	wing span
$\bar{c}$	=	reference chord length
C_D	=	drag coefficient
C_f	=	runway friction coefficient
C_L	=	lift coefficient
C_{L_0}	=	lift coefficient at zero angle of attack
C_{L_α}	=	lift slope
$C_{L_{\delta_e}}$	=	lift coefficient with elevator deflection
$C_{L_{\hat{q}}}$	=	lift coefficient with pitch rate
C_{l_β}	=	rolling-moment coefficient with sideslip angle
$C_{l_{\delta_a}}$	=	rolling-moment coefficient with aileron deflection
$C_{l_{\delta_r}}$	=	rolling-moment coefficient with rudder deflection
$C_{l_{\hat{p}}}$	=	rolling-moment coefficient with roll rate

*Graduate Researcher, ASDL, School of Aerospace Engineering, Georgia Tech, AIAA Student Member
†Senior Research Engineer, ASDL, School of Aerospace Engineering, Georgia Tech, AIAA Senior Member
‡S.P. Langley Distinguished Regents Professor and Director of ASDL, Georgia Tech, AIAA Fellow
§Assistant Professor, Department of Aerospace Engineering, Auburn University, AIAA Senior Member

$C_{l_{\hat{r}}}$ = rolling-moment coefficient with yaw rate
C_{m_0} = pitching-moment coefficient at zero angle of attack
C_{m_α} = pitching-moment coefficient with angle of attack
$C_{m_{\delta_e}}$ = pitching-moment coefficient with elevator deflection
$C_{m_{\hat{q}}}$ = pitching-moment coefficient with pitch rate
C_{n_β} = yawing-moment coefficient with sideslipe angle
$C_{n_{\delta_a}}$ = yawing-moment coefficient with aileron deflection
$C_{n_{\delta_r}}$ = yawing-moment coefficient with rudder deflection
$C_{n_{\hat{p}}}$ = yawing-moment coefficient with roll rate
$C_{n_{\hat{r}}}$ = yawing-moment coefficient with yaw rate
C_{Y_β} = side-force coefficient with sideslipe angle
$C_{Y_{\delta_a}}$ = side-force coefficient with aileron deflection
$C_{Y_{\delta_r}}$ = side-force coefficient with rudder deflection
$C_{Y_{\hat{p}}}$ = side-force coefficient with roll rate
$C_{Y_{\hat{r}}}$ = side-force coefficient with yaw rate
CG = center of gravity
D = drag
f = runway friction
I_{xx} = rolling mass moment of inertia
I_{yy} = pitching mass moment of inertia
I_{zz} = yawing mass moment of inertia
L = lift
p = roll rate
q = pitch rate
r = yaw rate
S = reference wing area
T = Thrust
u = body x-axis velocity
v = body y-axis velocity
V_∞ = airspeed
w = body z-axis velocity
W = weight

II. Introduction

Airworthiness certification is a fundamental safety requirement for all types of civil transportation aircraft. For a new aircraft or derivative aircraft, there are more than 1500 regulations that have to be verified by around 4000 tests and 16 000 demonstrations and inspections [1]. These test areas over flight performance, structure, design and construction, power plant, subsystems, etc. Due to the large number of regulations and tests, especially many of which must be verified by full scale testing demonstrations, the certification process can be time-consuming and expensive. Moreover, the certification cost is subject to uncertainty. A notional aircraft development process includes conceptual design, preliminary design, detailed design, prototype manufacturing, and testing. Under such a process, when the development moves to later stages, the design freedom diminishes, resulting in a significantly higher cost to make changes. However, in the notional design process, the certification check is not conducted until a later stage when there is little design freedom left. At that stage, if any necessary redesign has to be made for the compliance of certification requirements, the associated cost could be sufficiently high. To avoid the potential risk of increased costs, it is necessary to find an approach to shift certification considerations earlier in the design process.

III. Motivation

The motivation of this research originates from two aspects: 1. the design from new aircraft manufacturers; 2. the design of advanced novel concepts.

Existing large aircraft corporations, which have already double-oligarch monopolized the aviation market, rely on experience and historical data to predict the performance of airplane at early stages, trying to control uncertainty and

shorten certification period. However, for new aircraft manufacturers, the certification process might be challenging due to lack of experience. For example, Comac ARJ21 entered service eight years behind its original schedule due to certification delays [2]. The first delivery of Mitsubishi MRJ was delayed 5 times due to design changes needed for compliance with certification requirements [3]. These manufacturers have to afford the cost of redesign on top of the contractual costs at the risk of losing clients. As a result, certification has become a serious concern that discourages new aircraft manufacturers from entering the market.

The other motivating factor is the certification of advanced novel aircraft concepts. Due to the increasing restrictions on operational noise, fuel burn, emissions, and performance [4], new configurations and technologies are desired for future aircraft, such as hybrid wing-body, truss-braced wing, quiet supersonic jet, etc. Since these configurations and technologies are paradigm shifts from traditional aircraft design, the historical data and design experience may no longer be sufficient for the certification process of these novel aircrafts. These unconventional designs might be attractive in terms of environmental impacts and performance, but may pose unforeseen certification challenges. If the development process of new aircraft remains unchanged with certification considerations being enacted in later design stages, there is an unavoidable risk associated with the cost of certifying novel aircraft for both newcomers and existing aircraft manufacturers.

Therefore, in order to reduce the uncertainty, cost, and time spent on the certification process, there must be a way to incorporate certification considerations into early design stages. This relies on the technique of "virtual certification" in which the simulation environments from different disciplines are extensively used to check the certification constraints when designing an aircraft.

IV. Literature Review

The study on virtual certification initially started from the research on virtual flight testing. Previously, most research on virtual flight testing techniques were relied on ground experiment facilities, especially the wind tunnel [5, 6]. Consequently, those techniques may not be suitable for conceptual design since they are not parametric and require detailed information about the aircraft geometry. In relation to virtual flight testing in conceptual design, Georgia Tech's Aerospace Systems Design Lab (ASDL) developed a method of virtual flight testing for a supersonic prototype aircraft in 1998 [7] and created a virtual autonomous test and evaluation simulator for supersonic business jets in 2000 [8]. Despite their novelty, these methods and tools are only parametric for specific types of aircraft; thus, a well-defined approach linking virtual flight testing with certification is still missing.

In recent years, the significant cost on aircraft type certification has become a concern in aerospace industry. In 2011, the Advisory Council for Aviation Research and Innovation in Europe (ACARE) under the European Commission established the objective of reducing certification costs by 50% using "streamlined certification" in Flightpath 2050 Europe's Vision for Aviation [9]. Meanwhile, the European Union Aviation Safety Agency (EASA) regards the simulation-based virtual certification as one of their main focuses and identified the development and challenges associated with aircraft virtual certification [10]. Since then, some European institutions have launched several research efforts related to incorporating virtual certification with aircraft design based on different methods. For example, in the "Digital-X" project [11], German Aerospace Center (DLR) established a multidisciplinary platform for aircraft design and virtual flight test based on high-fidelity Computational Fluid Dynamics (CFD) and Finite Element Analysis (FEA). French Aerospace Laboratory and ISAE-SUPAERO developed a certification constraints module based on EASA CS-25 and incorporated with their own aircraft sizing code and flight dynamic model to yield a multidisciplinary analysis and optimization environment for aircraft conceptual design [12–14]. Aside from the incorporating certification with design, another way to reduce the certification cost is to replace flight tests by simulation and analysis, a.k.a. certification by analysis. The research effort on certification by analysis is focusing on the development of methods to maximize the use of numerical simulations in the certification process. For example, Georgia Tech's ASDL established a framework for structural dynamic load certification assessment [15]. Stanford University proposed a framework for certification maneuver simulation based on multi-fidelity aerodynamic analysis and uncertainty quantification [16]. Exa and Gulfstream developed a numerical procedure for the prediction of aircraft noise certification metrics [17]. Comac developed a certification analysis environment for wheels up landing certification [18] and bird strike certification [19] based on FEA.

It can be seen that most of the virtual certification research are based on high-fidelity analysis or experimental data. However, these methods may be impractical for early design stages due to the computational cost or lack of design knowledge. In terms of aircraft conceptual design, most of the efforts to date have been focusing on new concepts and design space exploration, while little attention is paid to certification. Admittedly, most clients are more interested in

performance, environmental impact, and cost, but certification is a basic requirement without which aircraft cannot be operated. In the academic domain, there are multiple Multidisciplinary Design Analysis and Optimization (MDAO) tools available for aircraft design, but very few of them are able to do certification analysis. While there are some certification analysis tools published, most of them are high-fidelity based which is not compatible to early design stage, and some of them are confined to specific configurations or sizing environments. A separate, general, robust, and parametric certification analysis environment for conceptual and early preliminary design is still needed.

V. Problem Formulation

The general goal of a certification analysis environment is to transform certification regulations to quantitative functions and connect with MDAO environment to constrain the sizing and optimization. However, it is impossible to check all the certification requirements at early design stage due to the lack of design knowledge. The checking process should be divided into multiple levels and allocated to different design stages based on the formulation of design knowledge, as presented in Figure 1.

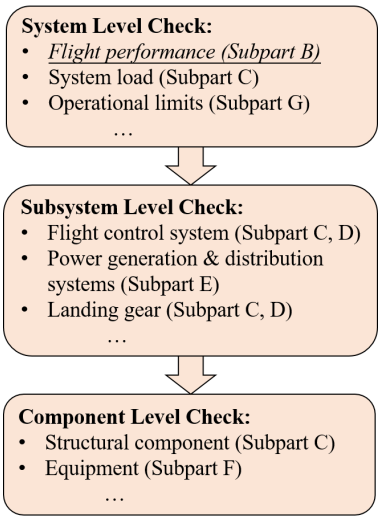

Fig. 1 Certification Check Levels

The system level check focuses on the responses of whole airplane, such as the aircraft flight performance, operational limits, and the load condition applied to the whole aircraft. The subsystem level check focuses on the operational performance of aircraft's subsystems, such as power plant, landing gear, avionics, flight control system, etc. The component level check focuses on the conditions of specific components and equipment in different parts of aircraft, such as the strength of structural components, the function and installation of flight instruments, etc. For a generalized certification analysis environment, the decomposition of certification checking process requires the environment to be decomposed to several modules, and each of these modules should correspond to a specific level of certification requirement checks. Yet in conceptual and early preliminary design, the subsystem level and component level checks are difficult to be performed since the details about subsystems and components are limited.

The development of generalized virtual certification analysis environment is laid over a multi-year plan. As a starting point, as well as the proof of concept of incorporating certification requirements into early design, this paper focused on the flight performance certification constraints check and developed a flight certification analysis module based on FAR-25 Subpart B Flight [20] and Advisory Circular AC 25-7D [21].

VI. Flight Certification Analysis Module

The flight certification analysis module checks the aircraft flight performance against certification regulations, including takeoff, climb, landing simulation, and flight dynamic analysis. The development of the module was conducted in MATLAB, in which each of the regulations that define specific constraints and metrics in FAR-25 Subpart B [20] is converted to a MATLAB function (regulation function). This guarantees that the execution of one regulation function is able to call any other regulation functions. The reason for such programming structure is that certification regulations

are cross-referenced; one regulation requirement check may need the information from other regulations. The structure of the flight certification analysis module is shown in Figure 2.

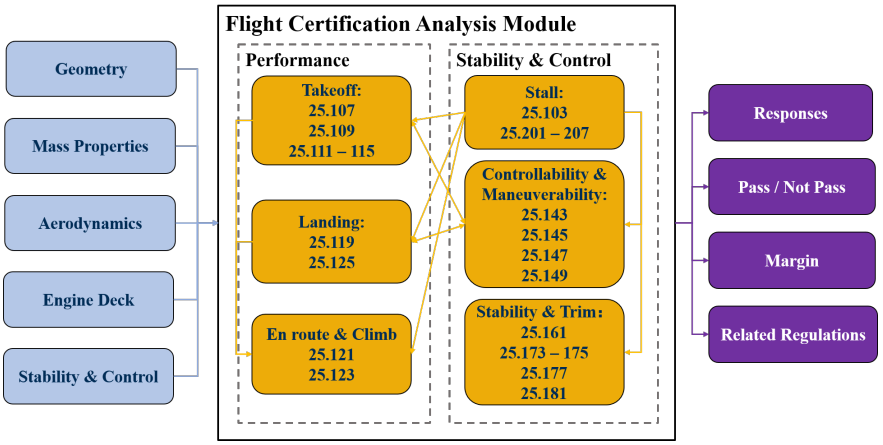

Fig. 2 Structure of Flight Certification Analysis Module

There are six components in the flight certification analysis module: takeoff, landing, climb, stall, controllability, and stability. Each component contains the MATLAB functions of corresponding regulations. These six components are correlated: the yellow arrows in Figure 2 indicate data transfer between regulation functions from various components, which represents the cross-referencing between regulations. Aside from regulation functions, a flight dynamic simulator based on six degree-of-freedom equations of motion is established within the certification module to support the regulation compliance check. One feature of the certification module is that all the aircraft-level analyses performed in the certification module are rigid-body based instead of point-mass based. The details about regulatory requirement modeling and flight dynamic simulator, as well as the input and output of the certification module are presented in following subsections.

A. Input

The input of the module is an aircraft digital model containing the information of geometry, mass properties, aerodynamics, propulsion, and stability and control. Geometry includes the dimensions and locations of components (i.e. wing, fuselage, horizontal tail, vertical tail, nacelle, etc.). Mass properties includes aircraft maximum takeoff gross weight (MTOW), maximum design landing weight (MDLW), reference CG location, CG envelope, and moments of inertia. Aerodynamics includes drag polars for takeoff, cruise, and landing configurations. Propulsion system information includes number of engines, sea level thrust, and a scalable engine deck. Stability & control includes aircraft longitudinal and lateral stiffness, damping rate, and control surface derivatives. The development of input model is not confined to any analysis tool or sizing environment; no matter low-fidelity approximations, or high-fidelity simulations, or even experimental data, all of them can be used to develop the input model.

One thing being noted is that current available conceptual design tools, such as NASA's Flight Optimization Software (FLOPS)[22, 23], are not able to provide all the information that the input model of certification module requires (e.g. stability & control derivatives, mass properties, etc.). In future works, additional analysis capabilities will be established to fill these gaps and integrated with the certification module. In this paper, some of the values in input model are based on low-fidelity approximation [24, 25].

B. Flight Dynamic Simulator

Because the regulations in FAR-25 Subpart B [20] specify the requirements on aircraft dynamic responses and maneuvering characteristics, the certification analysis cannot regard the aircraft as a point mass like traditional conceptual design methods. A dynamic flight simulator in the form of MATLAB function is established within the certification module, which can be called by any regulation function. The simulator is able to perform open-loop simulation, trim, and closed-loop control for all configurations (i.e. takeoff, cruise, and landing).

1. Equations of Motion

The dynamic simulator is developed based on six degree-of-freedom motion equations [26] and the body axes are assumed aligned with the principle axes for the simplification:

$$\begin{cases} \dot{u} = rv - qw + \frac{T+X_{aero}}{m} - g\sin\theta \\ \dot{v} = pw - ru + \frac{Y_{aero}}{m} + g\cos\theta\sin\phi \\ \dot{w} = qu - pv + \frac{Z_{aero}}{m} + g\cos\theta\cos\phi \end{cases} \tag{1}$$

$$\begin{cases} \dot{p} = \frac{L_{aero}+(I_{yy}-I_{zz})qr}{I_{xx}} \\ \dot{q} = \frac{M_{aero}+M_{thrust}+(I_{zz}-I_{xx})rp}{I_{yy}} \\ \dot{r} = \frac{N_{aero}+N_{thrust}+(I_{xx}-I_{yy})pq}{I_{zz}} \end{cases} \tag{2}$$

$$\begin{cases} \dot{\phi} = p + q\sin\phi\tan\theta + r\cos\phi\tan\theta \\ \dot{\theta} = q\cos\phi - r\sin\phi \\ \dot{\psi} = q\sin\phi\sec\theta + r\cos\phi\sec\theta \end{cases} \tag{3}$$

$$\begin{bmatrix} \dot{x}_e \\ \dot{z}_e \\ \dot{z}_e \end{bmatrix} = L_{bV} \begin{bmatrix} u \\ v \\ w \end{bmatrix} \tag{4}$$

where L_{bV} is the transformational matrix from NED frame to body frame. The aerodynamic forces and moments in Eqs. (1) and (2) are

$$\begin{cases} L = \frac{1}{2}\rho V_\infty^2 S(C_{L_0} + C_{L_\alpha}\alpha + C_{L_{\hat{q}}}\hat{q} + C_{L_{\delta_e}}\delta_e) \\ D = \frac{1}{2}\rho V_\infty^2 S C_D \\ X_{aero} = -D\cos\alpha\cos\beta + L\sin\alpha \\ Y_{aero} = \frac{1}{2}\rho V_\infty^2 S(C_{Y_\beta}\beta + C_{Y_{\hat{p}}}\hat{p} + C_{Y_{\hat{r}}}\hat{r} + C_{Y_{\delta_a}}\delta_a + C_{Y_{\delta_r}}\delta_r) \\ Z_{aero} = -L\cos\alpha - D\cos\beta\sin\alpha \end{cases} \tag{5}$$

$$\begin{cases} L_{aero} = \frac{1}{2}\rho V_\infty^2 Sb(C_{l_\beta}\beta + C_{l_{\hat{p}}}\hat{p} + C_{l_{\hat{r}}}\hat{r} + C_{l_{\delta_a}}\delta_a + C_{l_{\delta_r}}\delta_r) \\ M_{aero} = \frac{1}{2}\rho V_\infty^2 S\bar{c}(C_{m_\alpha}\alpha + C_{m_{\hat{q}}}\hat{q} + C_{m_{\delta_e}}\delta_e) \\ N_{aero} = \frac{1}{2}\rho V_\infty^2 Sb(C_{n_\beta}\beta + C_{n_{\hat{p}}}\hat{p} + C_{n_{\hat{r}}}\hat{r} + C_{n_{\delta_a}}\delta_a + C_{n_{\delta_r}}\delta_r) \end{cases} \tag{6}$$

To be clarified, L_{aero} is the roll moment generated by aerodynamic forces, while L is the lift. The pitch and yaw moment due to thrust alignment in Eq. (2) are

$$M_{thrust} = T \cdot z_N \tag{7}$$

$$N_{thrust} = \begin{cases} T \cdot y_N & \text{(critical engine inoperative)} \\ 0 & \text{(all engine operating)} \end{cases} \tag{8}$$

where y_N and z_N are the level arms between nacelle main axis and aircraft main axis in y and z directions.

The dynamic simulation is performed by numerically solving the six degree-of-freedom equations using the Euler's method. The whole flight process is discretized into a series of small time intervals assuming quasi-static process. The state variables at current time step are updated from the previous time step:

$$\begin{cases} \vec{u}_{i+1} = \vec{u}_i + \dot{\vec{u}}_i dt \\ \vec{\omega}_{i+1} = \vec{\omega}_i + \dot{\vec{\omega}}_i dt \\ \vec{x}_{i+1} = \vec{x}_i + \dot{\vec{x}}_i dt \end{cases} \tag{9}$$

2. Total Energy Control System (TECS)

The total energy control system (TECS) is integrated in the dynamic simulator for the vertical flight closed-loop simulation. The idea of TECS is to determine the throttle control δT_c and elevator control δ_{e_c} based on the flight path error γ_ϵ and acceleration error V_ϵ/g [27, 28]:

$$\delta T_c = (K_{TP} + \frac{K_{TI}}{S})(\gamma_\epsilon + \frac{V_\epsilon}{g}) \tag{10}$$

$$\delta_{e_c} = (K_{EP} + \frac{K_{EI}}{S})(\frac{V_\epsilon}{g} - \gamma_\epsilon) \tag{11}$$

where K_P is proportional gain and K_I is integral gain. For the simplification and fast evaluation, only proportional feedback control K_P is used in this paper. The application of TECS in certification module is explained in the following subsection.

C. Certification Requirements Modeling

1. Takeoff

FAR 25.105 to 25.115 describe the takeoff procedure and require the certification applicant to provide corresponding takeoff speeds, distances, and flight paths for both all engine operating and critical engine inoperative conditions at each weight, altitude, and ambient temperature within the operational limits [20]. In the certification module, the requirements are checked based on takeoff dynamic simulation. The takeoff process can be divided into several segments as shown in Figure 3 according to the Advisory Circular [21].

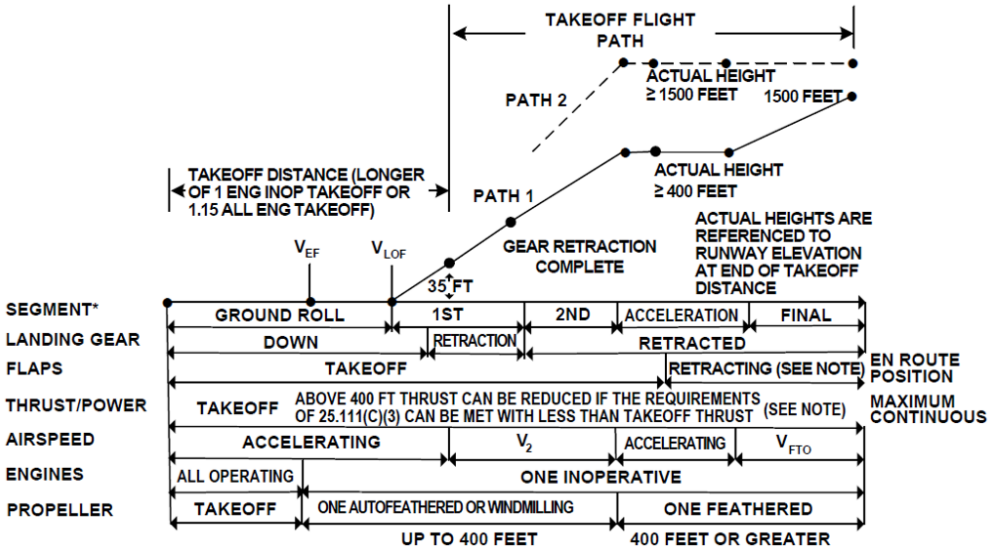

Fig. 3 Takeoff Segments and Nomenclature [21]

The ground roll segment can be divided into four sub-segments:

1) Accelerating from zero to engine failure velocity V_{EF}: V_{EF} is selected by applicant but constrained by minimum ground control speed V_{mcG}. The calculation of V_{mcG} is explained in Sec. VI.C.4.
2) Accelerating from V_{EF} to decision speed V_1 when the pilot notices the failure of engine and takes action. V_1 is calculated by

$$V_1 = V_{EF} + \int_0^{t_1} (T - D - f)\, dt \tag{12}$$

where t_1 is the time interval between engine failure and pilot's action.

3) Accelerating from V_1 to rotation speed V_R when the elevator control is able to balance the nose-down moment. V_R is solved by

$$M_{aero} + M_{thrust} - (W - L)(x_{MW} - x_{CG}) - C_f(W - L)(z_{CG} - x_{MW}) = 0 \tag{13}$$

where x_{CG}, x_{MW} and z_{CG}, z_{MW} are x-coordinates and z-coordinates of CG and main landing gear. M_{aero} and L are substituted from Eqs. (5) and (6), and M_{thrust} is substituted from Eq.(7). V_R is constrained by V_1 and minimum control speed V_{mc}. The calculation of V_{mc} is explained in Sec. VI.C.4.

4) Rotating the aircraft and accelerating to lift-off speed V_{LOF} when lift balances the takeoff weight. The rotation is constrained by the tail strike and stall angle of attack. In this paper, the elevator deflection during rotation is assumed as constant until one of the constraints is met.

The second segment is the takeoff climb after the aircraft becomes airborne. The takeoff climb analysis is performed by the flight dynamic simulator described in Sec. VI.B. Two procedures can be used for takeoff climb as shown in Figure 2:

1) Path 1: a level-off acceleration with the minimum gradient of climb specified in 25.111[20] at 400 feet is incorporated before climb to the height of 1500 feet;
2) Path 2: aircraft accelerates and climbs directly to 1500 feet above takeoff surface.

In this paper, path 2 is used for the takeoff with all engine operating since the excess power is sufficient for continues climb, while path 1 is used for the takeoff with critical engine inoperative. Because the retraction process of landing gear and flaps is difficult to be represented without detailed unsteady aerodynamic model, for the simplification, this paper regards the landing gear as a switch and assumes fully retracted at the height of 400 feet. The flap setting is assumed to be fixed at takeoff configuration until 1500 feet above the takeoff surface. During the takeoff climb, the maximum climb angle is desired for the obstacle clearance in the first (0 to 35 feet) and second (35 to 400 feet) takeoff climb segments, and the maximum rate of climb is desired for the minimum time to climb in the final (400 to 1500 feet) takeoff climb segment. In the takeoff climb analysis, two trimmed condition are computed from the flight dynamic simulator in advanced of dynamic simulation: one is the maximum climb angle condition at 400 feet above the takeoff surface, the other is the maximum rate of climb condition at 1500 feet above the takeoff surface. The TECS introduced in Sec. VI.B.2 is used to determine the elevator control during the takeoff climb dynamic simulation in order to make the aircraft match these two desired flight conditions as closed as possible. The takeoff safety speed V_2 at 35 feet above takeoff surface and the final takeoff speed V_{FTO} at 1500 feet above takeoff surface are computed from the dynamic simulation. V_2 is checked against the stall speed constraint and V_{mc} constraint as specified in 25.107 [20].

The takeoff path, takeoff distance, and takeoff net flight path as defined in 25.111, 25.113, and 25.115 [20] are computed from the takeoff dynamic analysis. For rejected takeoff, 25.109 requires the aircraft to perform the accelerate-stop distance test on both dry runway and wet runway. For the wet runway test, the runway braking coefficient is determined by multiplying the anti-skid system efficiency specified in 25.109(c)(2) [20] with the maximum braking coefficient defined in 25.109(c)(1) [20]. Figure 4 extracted from the Advisory Circular [21] depicts the decomposition of accelerate-stop distance.

2. Climb

The climb constraints in certification regulation are defined in terms of minimum gradient of climb, which equals to the tangent of minimum climb angle. Specifically, 25.119 defines the minimum gradient of climb for landing go-around condition [20], and 25.121 defines the minimum gradient of climb with critical engine inoperative at takeoff, cruise, and landing configurations [20]. In certification module, climb constraints are checked by comparing the maximum available gradient of climb against the constraint values. The maximum available gradient of climb is computed by longitudinal trim analysis using flight dynamic simulator, in which the maximum available thrust is identified from the engine deck and the flight path angle is computed from the climb trim.

3. Landing

FAR 25.125 describes the landing procedure and requires the applicant to provide the landing distance and the landing reference speed V_{REF}. In certification module, landing constraints are checked by landing dynamic simulation. The landing process can be divided into four segments: stabilized approach, flare, touchdown and brake:

1) Stabilized approach: aircraft approaches the runway in a manner of steady descent with the approach speed V_{app} and -3° flight path angle. V_{app} is approximated from V_{REF}, which is computed by

$$V_{REF} = 1.3V_{SR} \tag{14}$$

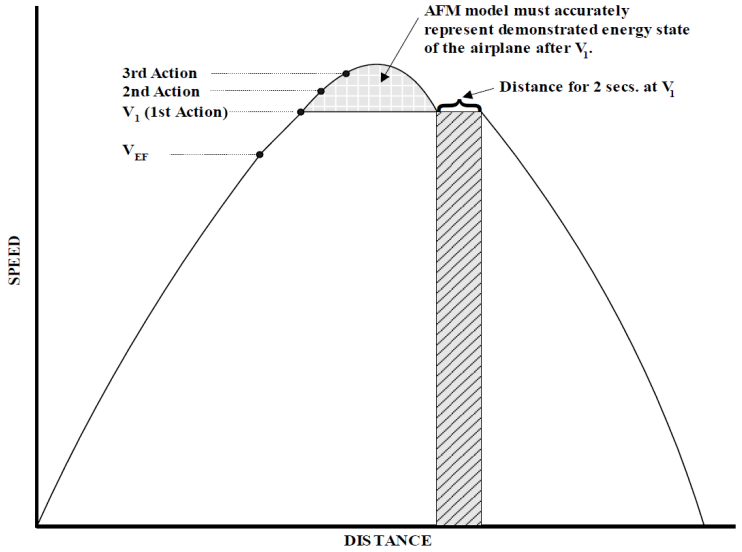

Fig. 4 Accelerate-Stop Speed versus Distance [21]

$$V_{app} = V_{REF} + \Delta V_{app} \tag{15}$$

where V_{SR} is the reference stall speed and ΔV_{app} is the delta approach velocity. The trimmed condition for stabilized approach is computed by the flight dynamic simulator.

2) Flare: aircraft starts to reduce thrust and pitch up at flare height. The thrust is assumed to be linearly decreased from stabilized approach setting to idle within two seconds. The elevator control in flare segment is determined by the TECS introduced in Sec. VI.B.2 to pitch up the aircraft and decrease the rate of descent at touchdown, thus to encourage a smooth landing. According the Advisory Circular [21], the rate of descent at touchdown should not be higher than 6 feet per second.
3) Touchdown: the main landing gear touches runway while the nose landing gear remains airborne. In this segment, it is assumed that spoiler is the only decelerating action being deployed until the touchdown of nose landing gear. The bounce effect is not included in the simulation.
4) Brake: the nose landing gear touches runway and full brake is deployed. The reserved thrust, which is modeled as 40% of maximum available thrust, is assumed activated until 80 knots.

The landing distance defined as the horizontal distance from 50 feet obstacle height to fully stopped [20] is computed from the dynamic simulation.

4. Controllability and Maneuverability

The controllability and maneuverability includes five aspects: controllability following engine failure, constant speed coordinated turn, longitudinal control, lateral & directional control, and minimum control speed. Note that the qualitative controllability requirements are not covered in the certification module.

FAR 25.143(b) requires that the transition from sudden failure of the critical engine should be smooth. Correspondingly, two maneuvers are specified in the Advisory Circular to show the compliance with this requirement [21]: 1. At takeoff flap setting and initial all-engine climb speed, once the critical engine fails, no recovery action is applied until two-second delay; 2. Perform the same procedure at cruise configuration and $1.23V_{SR}$. During the maneuver process, the bank angle should not exceed 45° [21]. In the certification module, The simulation of maneuvers is performed by the flight dynamic simulator. The aircraft lateral attitudes are tracked in the simulation. The requirement is checked by comparing the maximum bank angle with constraint value.

FAR 25.143(h) requires the aircraft to perform a constant speed coordinated turn in the following four scenarios [20]: takeoff configuration with asymmetric thrust ($\phi = 30°$), takeoff climb with all engine operating ($\phi = 40°$), cruise configuration with asymmetric thrust ($\phi = 40°$), and landing configuration with symmetric approach thrust ($\phi = 40°$). The coordinated turn must be free of stall and the control surfaces must be able to provide sufficient control power to sustain the turn. To check the constraint, the trimmed condition for coordinated turn is computed from the flight

dynamic simulator by solving Eqs. (1) and (2), where the angular velocity is calculated from the bank angle and velocity specified in the regulation [26]:

$$\dot{\psi} = \frac{g \tan \phi}{V} \tag{16}$$

$$\begin{bmatrix} p \\ q \\ r \end{bmatrix} = \begin{bmatrix} -\theta \\ \sin \phi \\ \cos \phi \end{bmatrix} \dot{\psi} \tag{17}$$

α, β, δ_a, δ_e and δ_r are solved from the coordinated turn trimmed condition. The certification constraint is checked by comparing α against the stall angle of attack, and comparing δ_a, δ_e and δ_r against the maximum allowable control surface deflections.

FAR 25.145 defines the longitudinal control requirements in two aspects [20]: 1. The controllability to pitch down aircraft recovering from stall; 2. The controllability to prevent loss of height and velocity during the change of thrust and flap setting. The stall recovery check is not included in this paper because the simulation on stall requires high-fidelity unsteady aerodynamic analysis. For the longitudinal controllability during configuration change, due to the lack of aerodynamic model for flap transition process, the dynamic longitudinal controllability check is not included in this paper either. But instead, the static longitudinal analysis at four boundary conditions (extended flaps with/without thrust, retracted flaps with/without thrust) are temporarily used for constraint check. Four trimmed points are computed from the flight dynamic simulator. Based on the difference on θ between two flight conditions, an average pitch rate is approximated from the time taken for configuration change. The constraint is checked by the magnitude of the average pitch rate.

FAR 25.147 and the Advisory Circular requires the aircraft to perform three maneuvers to demonstrate the lateral and directional controllability [20, 21]: 1. A sudden change in heading of up to 15 degrees in the direction of the critical inoperative engine; 2. A 20-degree banked coordinated turn with maximum asymmetric thrust; 3. Starting from a 30° banked coordinated turn with maximum asymmetric thrust at V_2, roll to a 30° bank angle in the other direction within 11 seconds. All of these maneuvers are performed using the dynamic simulator. For the first maneuver, maximum rudder deflection is applied and aileron control is used to maintain the level flight. The aircraft attitudes and control surfaces deflections are tracked in the simulation. For the second maneuver, the coordinated turn constraint check is same as the checking process described for 25.143(h) above. For the third maneuver, a trimmed turn condition at V_2 is established in the flight dynamic simulator as a starting point. Then the maximum aileron deflection is applied to roll the aircraft and rudder control is used to minimize the sideslip. The aircraft attitudes and control surface deflections, as well as the time to perform maneuver, are tracked in the dynamic simulation.

FAR 25.149 requires the applicant to provide the minimum control speed V_{mc}, the minimum control speed at ground V_{mcG}, and the minimum control speed during landing approach V_{mcL} [20]. In the certification module, V_{mcG} is computed by

$$\frac{1}{2}\rho V_{mcG}^2 Sb(C_{n_{\delta_r}} \delta_{r_{max}}) - N_{thrust} + n_f = 0 \tag{18}$$

where N_{thrust} is substituted from Eq. (8). n_f is the sum of external yaw moment produced by the friction of landing gear. V_{mc} and V_{mcL} are solved from steady sideslip equations [26]:

$$\begin{cases} Y_{aero} + mg \cos \gamma \phi = 0 \\ L_{aero} = 0 \\ N_{aero} + N_{thrust} = 0 \end{cases} \tag{19}$$

where ϕ cannot be larger than 5° as required by 25.149(b)(f) [20], and Y_{aero}, L_{aero}, and N_{aero} are substituted from Eqs. (5) and (6) with angular velocity equal to zero. Additionally, the regulation requires the aircraft to perform the recovery from engine failure and other specific maneuvers at minimum control speeds to demonstrate the controllability. The constraints associated these maneuvers are also defined in 25.149(d)(e)(h) [20]. For V_{mc}, the heading angle change during the recovery should be less than 20°. For V_{mcG}, the path deviation from the centerline of ground roll should be less than 30 feet. For V_{mcL}, the lateral control should be able to roll the aircraft to 20° bank angle in the direction away from inoperative engine. All of these maneuver constraints are checked using the flight dynamic simulator, except for the path deviation check since it requires detailed information about landing gear system.

5. Stability and Trim

FAR 25.161 specifies the critical flight conditions for trim test [20]. The trim analysis is performed by the flight dynamic simulator. α, β, δ_a, δ_e and δ_r are solved from the trim analysis and compared with critical values.

FAR 25.173 to 25.181 defines the static and dynamic stability requirements [20], which are checked by eigen-mode analysis in certification module:

$$\dot{X} = AX + BU \tag{20}$$

where X and U are state and control vectors. A and B are derivative matrices. For the open loop analysis, the eigen-mode analysis is applied on A. In certification module, the derivatives in A matrix are numerically calculated by the flight dynamic simulator. The stability constraint is checked by the sign of the real part of the eigenvalues of A.

6. Stall

Stall includes two aspect: stall speed and stall recovery. The reference stall speed V_{SR} is specified in FAR 25.103 [20], which is computed by

$$V_{SR} = \sqrt{\frac{2n_{ZW}W}{\rho S C_{L_{max}}}} \tag{21}$$

where n_{ZW} is the load factor normal to the flight path at $C_{L_{max}}$. At different combinations of configuration and flight condition, V_{SR} are different.

The stall recovery requirements and testing procedures are specified in 25.201 to 25.207[20]. However, as mentioned in previous section, the stall recovery check is difficult to perform at early design stage due to the non-linear nature of aerodynamics and flight dynamics in stall recovery process. Because there is no such stall aerodynamic and flight dynamic model available for conceptual design, the stall recovery analysis is not included in this paper. In future works, additional analysis capability might be developed to fulfill such gap.

D. Output

The analysis results from the certification module not only indicate the compliance with requirements, but also present the aircraft responses values and the margin with respect to the constraint specified in regulations. Additionally, the related regulations and corresponding check results are included in the output. One feature of the module is that the module does not use constraint violation as a exit criteria, but instead informs the designer by showing the margin and asks the designer to decide whether a design change is needed. The reason is that in early design stage, there are many uncertainties due to analysis fidelity or the lack of design knowledge. It is difficult to tell whether a certification check failure is caused by the design scheme or by incontrollable uncertain factors.

E. Validation

To demonstrate the capability and evaluate the accuracy of the flight certification analysis module, a Small Single-aisle Aircraft (SSA) model calibrated using the data of Boeing 737-800 from Integrated Subsystems Sizing and Architecture Assessment Capability (ISSAAC)[29] is used to create the testing model. The stability and control derivatives are computed using AVL [25]. The moments of inertia are approximated based on Roskam [24]. The CG envelope is derived from the landing gear loading on pavement of Boeing 737-800 [30], as shown in Figure 5. The key performance and geometry specifications of the testing model are shown in Table 12 in Appendix. The analysis results from certification module are compared with public domain data of 737-800 [30, 31].

VII. Results and Discussion

A. Certification Constraint Check Result

1. Takeoff

The takeoff certification analysis results are shown in Table 1, and Figure 6 to 9. Table 1 shows the check results of takeoff speed constraints at MTOW and sea-level runway. The check result includes takeoff speed values, associated constraints and compliance status, the margin with respect to constraint (not shown in table due to limited space), as well as the regulations cross-referenced by 25.107 [20]. Figure 6 and Figure 7 are from the takeoff dynamic simulations with

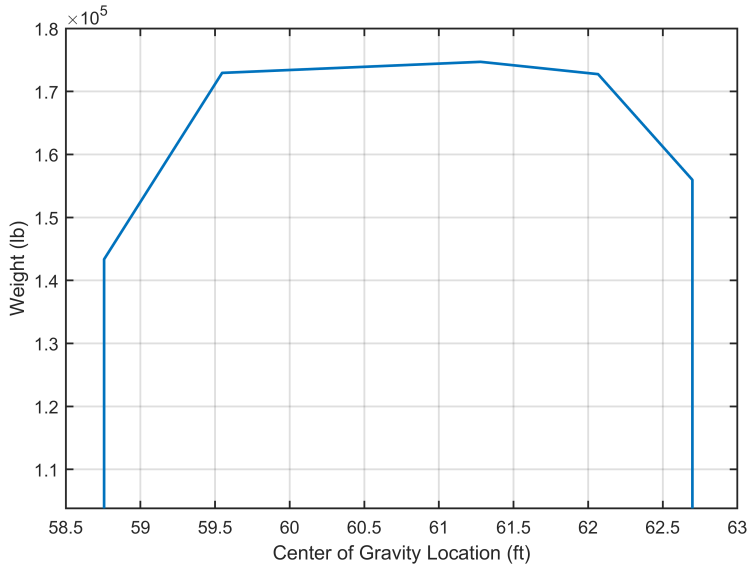

Fig. 5 CG Envelope of the Testing Model

all engine operating and critical engine inoperative, where Figure 6 shows the takeoff velocity change with respect to time and Figure 7 displays the takeoff path. The dash lines in Figure 7 are the net takeoff flight path which is defined as the actual flight path diminished by a gradient of climb according to 25.115 (b) [20]. Comparing the horizontal distance of takeoff path and the total time spent on takeoff between all-engine-operating and one-engine-out scenarios, it can be seen that the performance penalty from one-engine out is significant. Figure 8 shows the capability of certification module on performing takeoff dynamic simulation at different altitudes, weights, and CG locations, as required by 25.105 [20]. The left plot is similar to the takeoff performance plot contained in aircraft flight manual (AFM), which indicates the takeoff field length at different combinations of weights and runway altitudes. The CG location used in the left plot is fixed at the reference point. The right plot displays the takeoff distance at different combinations of weights and CG locations in the form of a contour in CG envelope. The runway altitude used for right plot is fixed at sea level. Figure 9 shows the accelerate-stop distance test result in the form of speed versus distance plot corresponding to the Figure 4 from Advisory Circular [21]. The simulation is performed based on both dry runway and wet runway. The blue dash lines in Figure 4 followed the procedure described in 25.109(a)(1) [20], in which the engine fails at V_{EF} and pilot takes the first action at V_1. The orange solid lines followed the procedure described in 25.109(a)(2) [20], in which all engines operating to the highest speed reached during the rejected takeoff and pilot rejected takeoff at V_1.

Table 1 25.107 Takeoff Speeds Certification Constraint Check

Metric	Value (knot)	Constraint	Pass	Related Regulations	Metric	Value (knot)
V_{EF}	130.67	$V_{EF} > V_{mcG}$	Yes	25.149	V_{mcG}	91.72
V_1	132.45					
$V_{2_{min}}$	118.94	$V_{2_{min}} > 1.3V_{SR}$	Yes	25.103	V_{SR}	112.08
		$V_{2_{min}} > 1.1V_{mc}$	Yes	25.149	V_{mc}	108.13
V_2	145.06	$V_2 > V_{2_{min}}$	Yes	25.143	30° Turn	Pass
V_R	132.49					
V_{LOF}	141.25					
V_{FTO}	186.11					

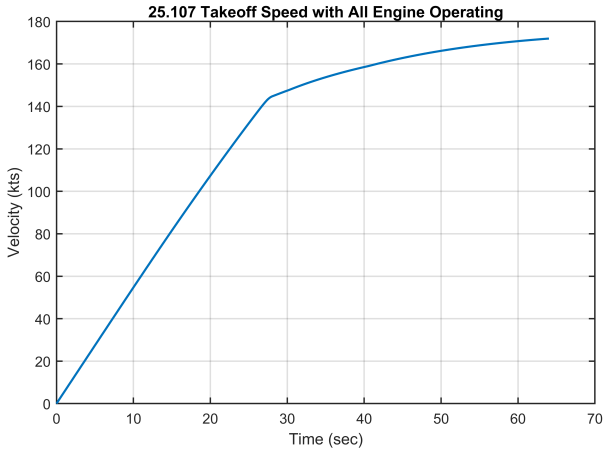

(a) All Engine Operating

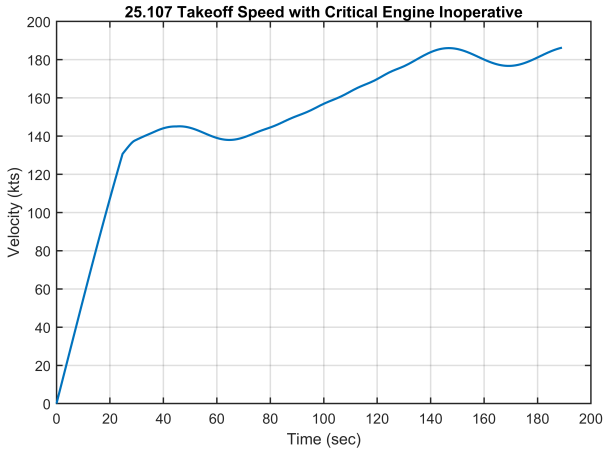

(b) Critical Engine Inoperative

Fig. 6 25.107 Takeoff Velocity

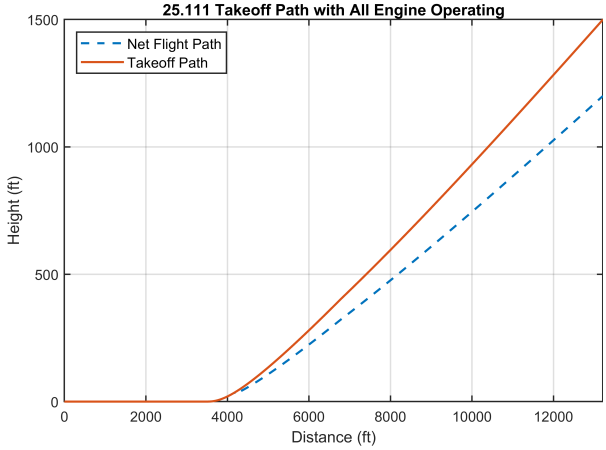

(a) All Engine Operating

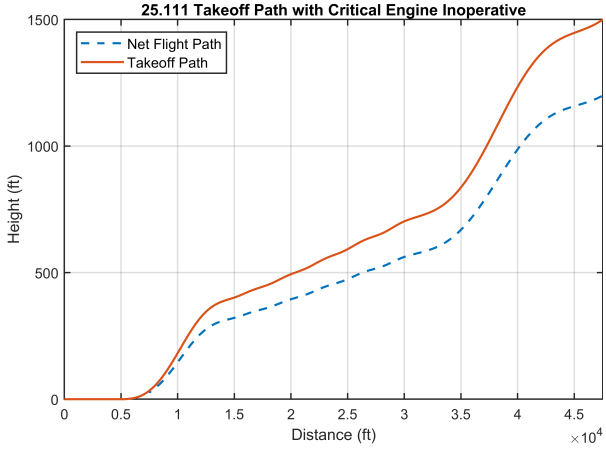

(b) Critical Engine Inoperative

Fig. 7 25.111 Takeoff Path

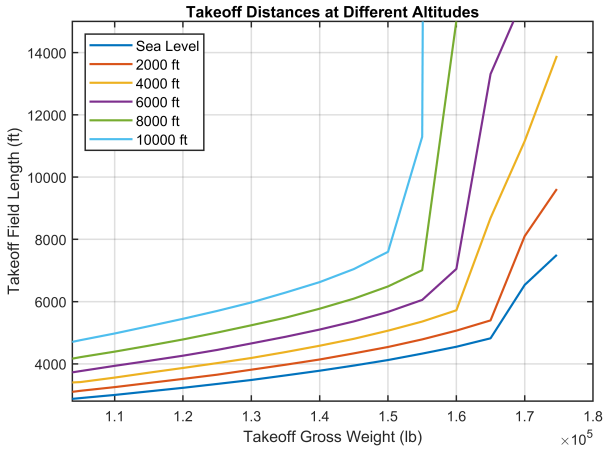

(a) Change with Altitude and Weight

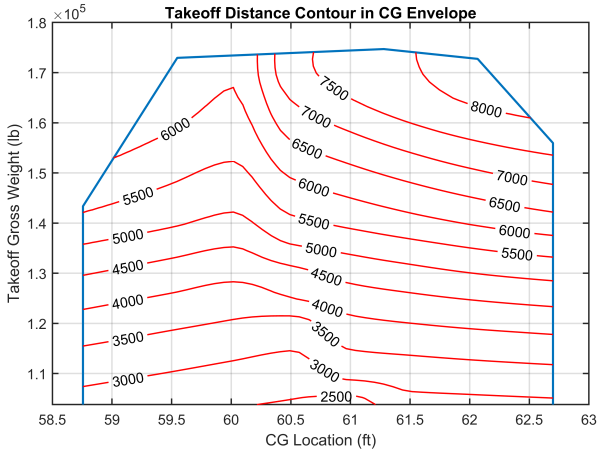

(b) Change with of Weight and CG

Fig. 8 25.113 Takeoff Distance

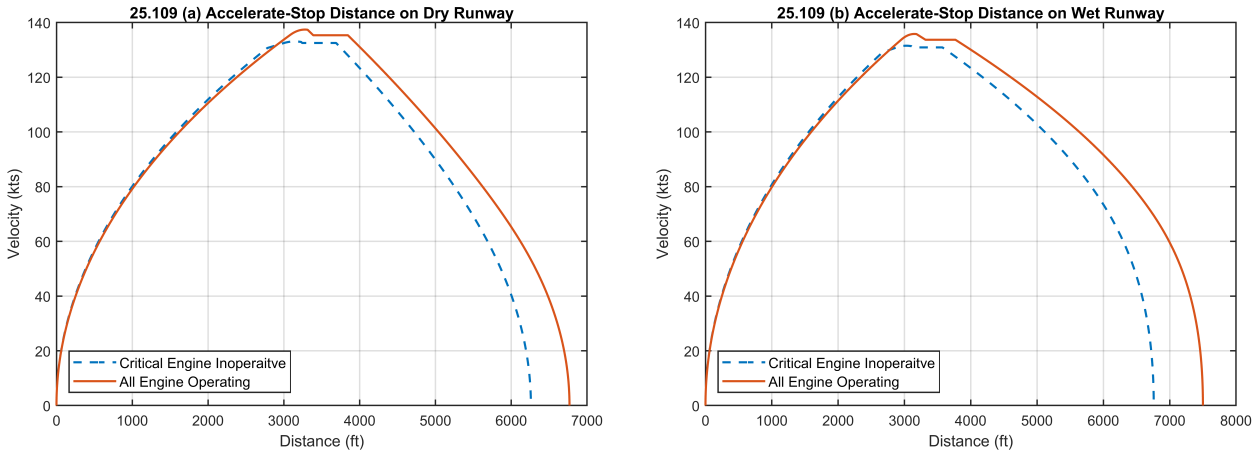

(a) Dry Runway (b) Wet Runway

Fig. 9 25.109 Accelerate-Stop Distance

2. Climb

The climb certification analysis results are shown in Table 3. MTOW is used for takeoff and cruise configurations tests, and MDLW is used for landing configuration tests. The thrust setting for 25.119 check is the go-around with all engine operating, while the thrust setting for 25.121 check is the maximum available thrust with critical engine inoperative. Comparing the margin with respect to minimum gradient of climb constraint, the landing configuration climb with critical engine inoperative is the most critical condition for climb certification.

Table 2 25.119 & 25.121 Climb Certification Constraint Check

Regulation	Configuration	Velocity	Gradient of Climb	Constraint	Pass
25.119	Landing	V_{REF}	0.202	> 0.032	Yes
25.121	Takeoff (with Landing Gear)	V_{LOF}	0.013	> 0	Yes
	Takeoff (w/o Landing Gear)	V_2	0.046	> 0.024	Yes
	Cruise	V_{FTO}	0.051	> 0.012	Yes
	Landing	$1.4V_{SR}$	0.033	> 0.021	Yes

3. Landing

The landing certification analysis results are shown in Table 3, and Figure 10 to 12. Table 3 indicates the check results of the constraints on approach reference speed, touchdown rate of descent, and flare control power at MDLW and sea-level runway. The corresponding dynamic simulation is shown in Figure 10 and Figure 11. Figure 10 presents the landing path and the landing velocity starting from 50 feet above landing surface to fully stop. The sequence of the deployment of deceleration actions (i.e. spoiler, reverse thrust, and brake) can be identified from the velocity plot. Figure 11 shows the aircraft longitudinal attitudes and elevator control from starting point to the point when the nose landing gear touches ground. The maximum elevator deflection (absolute value) extracted from the elevator control plot is used for the flare control power check. Such deflection is compared with the maximum allowable elevator deflection to determine whether the elevator needs to be resized. Similar to the takeoff simulation, Figure 12 shows the capability of certification module on analyzing the landing performance at different altitudes, weights, and CG locations.

4. Controllability and Maneuverability

The certification analysis result on controllability following engine failure is shown in Figure 13. The two plots in Figure 13 shows the aircraft lateral responses following the maneuver specified in the Advisory Circular [21] as

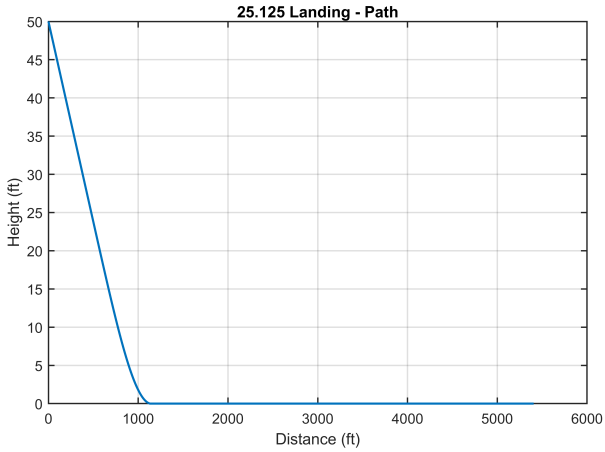

(a) Landing Path

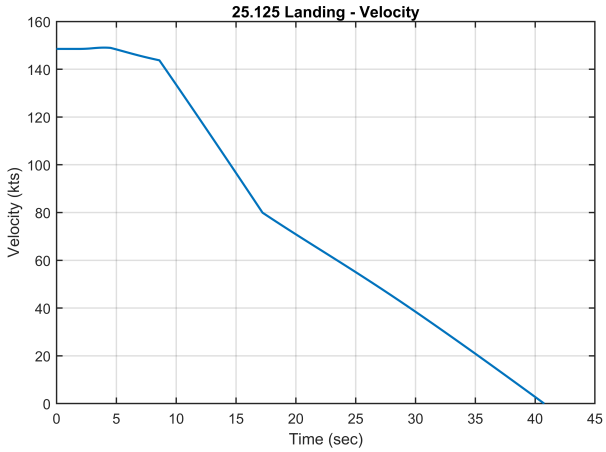

(b) Landing Velocity

Fig. 10 25.125 Landing Path and Velocity

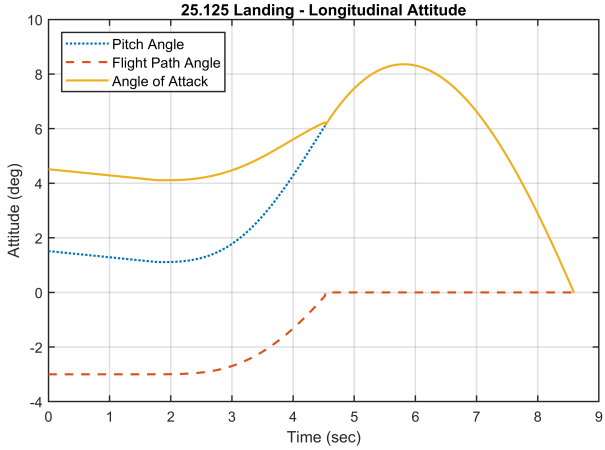

(a) Longitudinal Attitude

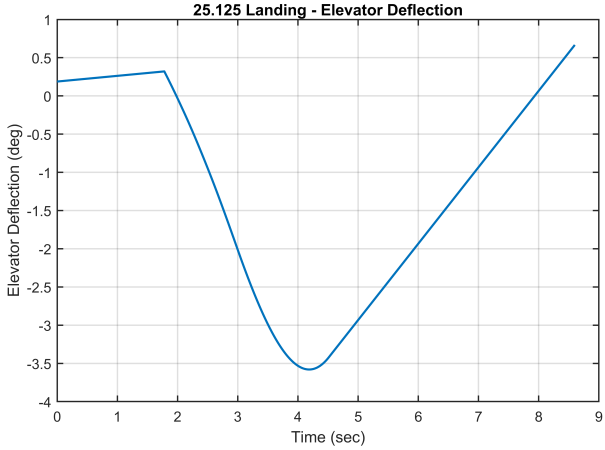

(b) Elevator Control

Fig. 11 25.125 Landing Dyanmic Simulation

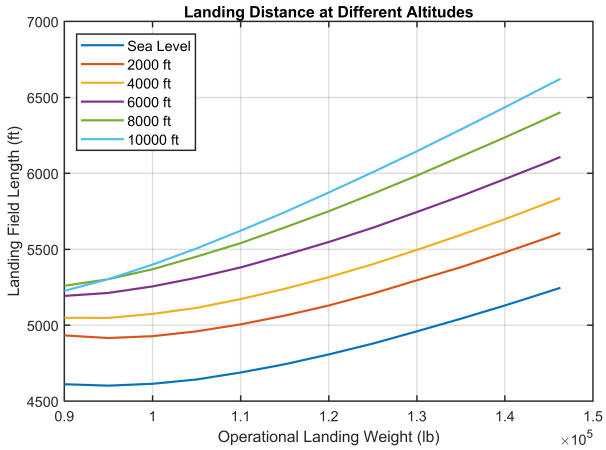

(a) Change with Altitude and Weight

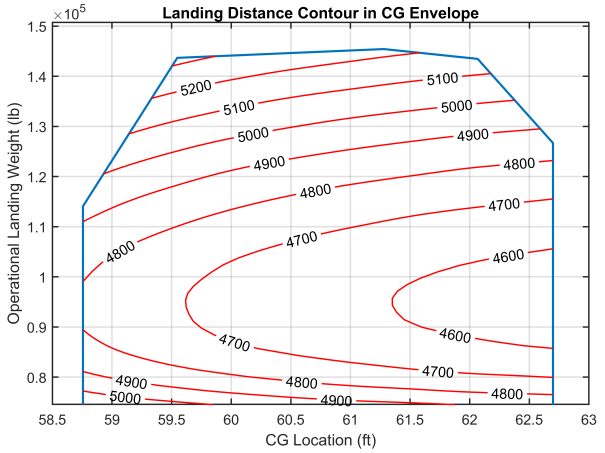

(b) Change with Weight and CG

Fig. 12 25.125 Landing Distance

Table 3 25.125 Landing Certification Constraint Check

Metric	Value	Constraint	Pass	Related Regulations	Metric	Value
V_{REF}	138.51 kts	$V_{REF} > 1.23V_{SR}$	Yes	25.103	V_{SR}	98.86 kts
		$V_{REF} > V_{mcL}$	Yes	25.149	V_{mcL}	103.35 kts
				25.143	40° Turn	Pass
Rate of Descent	−0.52 ft/s	$V \sin\gamma > -6$ ft/s	Yes			
Flare δ_e	−3.58°	$\lvert\delta_e\rvert < \delta_{e_{max}}$	Yes			

mentioned in Sec.VI.C.4. The maximum bank angles of two cases are less than 45° which satisfy the constraint. Comparing the deviations of roll and yaw attitudes from initial trim point, the takeoff flap setting case is more critical than the retracted flap cases.

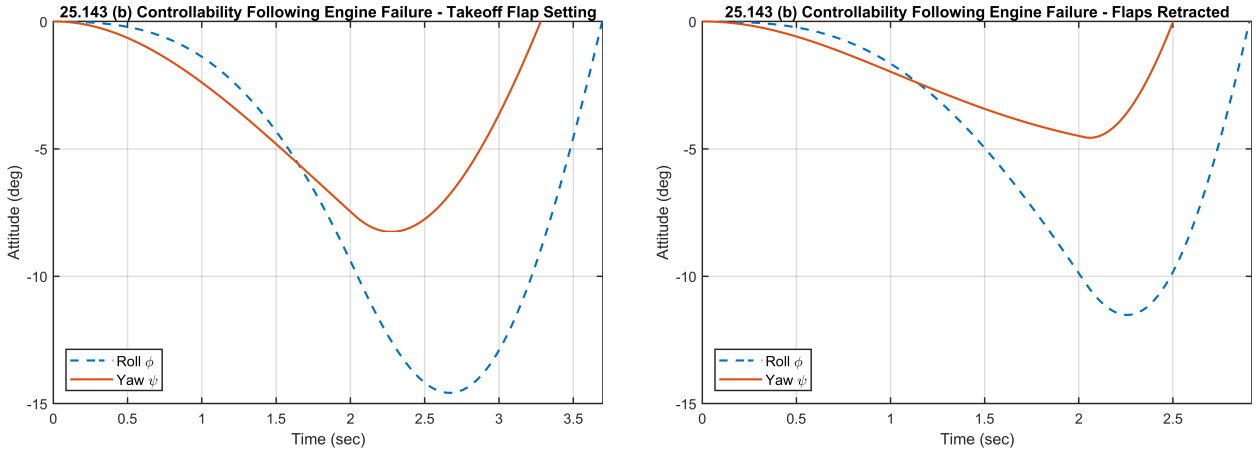

(a) Takeoff flap setting

(b) Flaps retracted

Fig. 13 25.143(b) Controllability Following Engine Failure

The constant speed coordinated turn certification analysis results are shown in Table 4. The aircraft attitudes and control surface deflections to sustain the coordinated turn at these four flight conditions are computed from the trim analysis using the flight dynamic simulator. The result indicates that the coordinated turn at takeoff configuration with critical engine inoperative is the most critical case to rudder control. All these four cases also constrain the aircraft stall characteristics according to the angle of attack required to maintain the coordinated turns.

Table 4 25.143(h) Coordinated Turn Certification Check Result

Configuration	Velocity	ϕ	α	β	δ_e	δ_r	δ_a
Takeoff (Asymmetric Thrust)	V_2	30°	14.26°	-6.53°	-10.97°	-18.42°	-10.07°
Takeoff (Symmetric Thrust)	$V_2 + 10$	40°	15.25°	-5.57°	-11.09°	-8.59°	-12.74°
Cruise (Asymmetric Thrust)	V_{FTO}	40°	11.12°	-3.44°	-11.73°	-9.30°	-4.85°
Landing (Symmetric Thrust)	V_{REF}	40°	11.41°	0.37°	-8.64°	-1.87°	-0.92°

The longitudinal controllability certification analysis result are shown in Table 5. Trim analysis is performed at different combinations of flap and thrust settings. The controllability is checked by the average pitch rate and the difference in elevator deflections since the flaps transition model is not available. The average pitch rate is computed by the difference in θ divided by the approximated time to perform the maneuver specified in Table 5.

Table 5 25.145 Longitudinal Control Certification Check Result

Configuration	α	γ	θ	δ_e
Flaps Retracted with Power Off	3.88°	-2.07°	1.80°	-3.76°
Flaps Extended with Power Off	9.55°	-7.16°	2.39°	-7.61°
Flaps Retracted with Maximum Power	3.76°	8.18°	11.94°	-1.14°
Flaps Extended with Maximum Power	8.98°	5.59°	14.57°	2.00°

Maneuver	Average Pitch Rate	Difference in δ_e
Extend Flaps (Power Off)	0.03	-3.85°
Retract Flaps (Power Off)	-0.03	3.85°
Retract Flaps (Go-around Power)	0.51	-3.15°
Idle to Maximum Thrust (Flaps Retracted)	2.03	2.62°
Idle to Maximum Thrust (Flaps Extended)	2.44	9.62°

The lateral & directional controllability certification analysis results are shown in Figure 14, Figure 15, and Table 6. Figure 14 shows the dynamic simulation of yawing into the inoperative engine from trimmed condition as specified in 25.147(a) [20]. Maximum rudder control is applied to yaw the aircraft until heading change up to 15°, and the aileron control is used to minimize the bank deviation. The directional controllability is measured by the time to perform the maneuver. Table 6 indicates the aircraft attitudes and control surface deflections required to perform 20° banked turn at $1.3V_{SR}$ and MTOW with critical engine inoperative. Figure 15 shows the dynamic simulation of rolling to 30° bank angle in the opposite direction from 30° banked steady turn as specified in the Advisory Circular [21], where maximum aileron control is applied to roll the aircraft from $-30°$ to 30° bank, and the rudder and elevator controls are used to minimize the sideslip and maintain pitch attitude. In Figure 15, the control surface deflections are assumed changing instantaneously from steady turn trimmed condition to roll maneuver condition at the starting point. The time to perform the maneuver is less than 4 seconds, which satisfy the constraint of less than 11 seconds [21].

Table 6 25.147(c) Lateral Control: 20° Banked Coordinated Turn

Configuration	Velocity	ϕ	α	β	δ_e	δ_r	δ_a
Takeoff (Asymmetric Thrust)	$1.3V_{SR}$	20°	11.59°	-4.98°	-4.49°	-13.58°	-7.38°

The minimum control speed certification analysis results are shown in Table 7 and Figure 16. Table 7 indicates the values of minimum control speeds computed from the certification module. V_{mc} is checked against the reference stall speed as specified in 25.149(c) [20]. Figure 16 shows the dynamic simulation of maneuverability constraint check at minimum control speeds. The left plot shows the recovery process from critical engine failure at V_{mc}, in which the maximum handing change cannot be larger than 20°. The right plot shows maneuver simulation following the procedure described in 25.149(h) [20], in which the aircraft must roll to 20° in the direction to initiate a turn away from the inoperative engine within five seconds.

Table 7 25.149 Minimum Control Speeds

Metric	Value (knot)	Constraint	Pass	Related Regulations	Metric	Value (knot)
V_{mc}	108.13	$V_{mc} < 1.13V_{SR}$	Yes	25.103	V_{SR}	112.08
		$\Delta\psi < 20°$	Yes			
V_{mcG}	91.72	Path deviation	NA			
V_{mcL}	103.35	Roll capability	Yes			

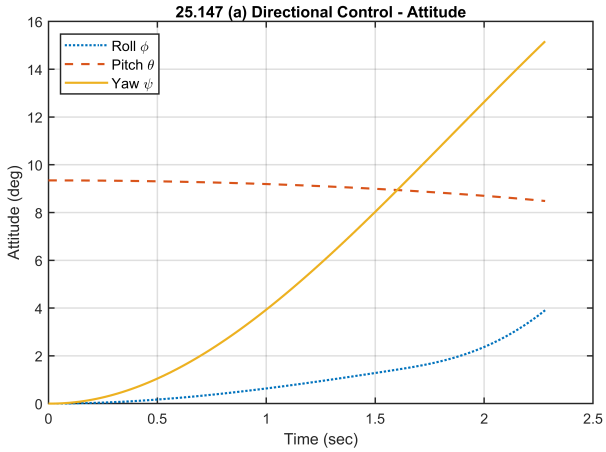

(a) Attitudes

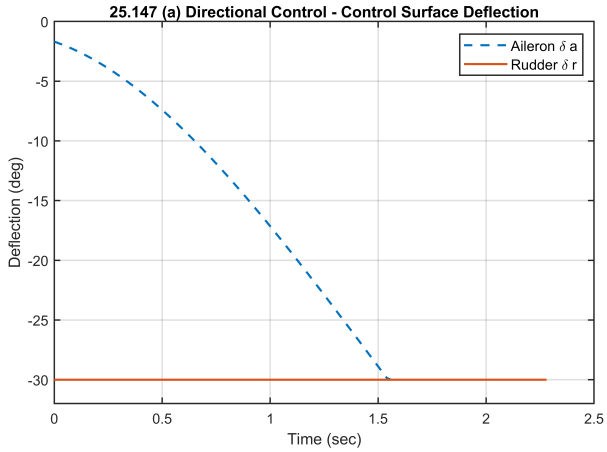

(b) Control Surfaces

Fig. 14 25.147(a) Directional Control: Sudden Change in Heading Angle

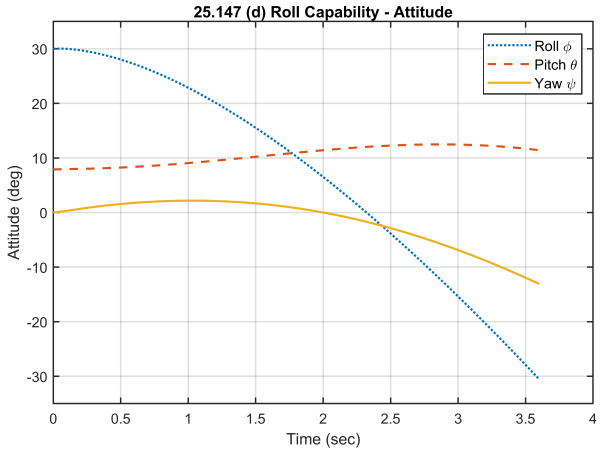

(a) Attitudes

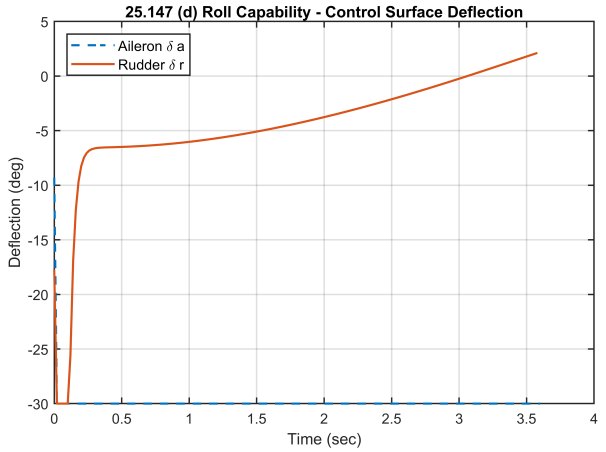

(b) Control Surfaces

Fig. 15 25.147(d) Lateral Control: Roll Capability

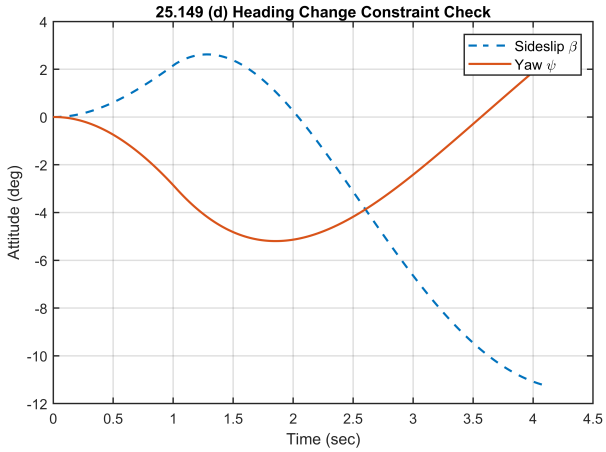

(a) 25.149(d) Heading Angle Deviation

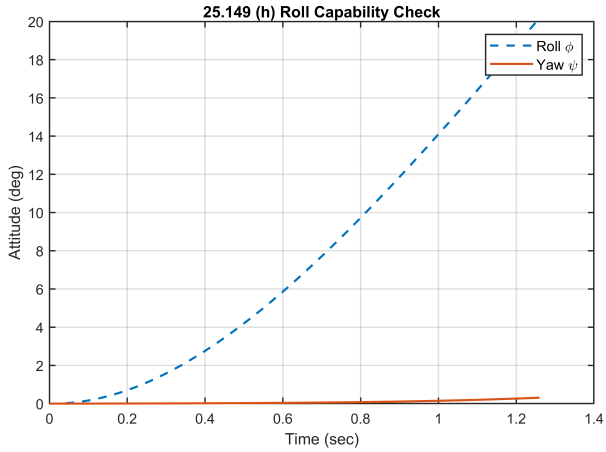

(b) 25.149(h) Roll Capability

Fig. 16 25.149 Minimum Control Speeds Certification Constraint Check

5. Stability and Trim

The trim certification analysis results are shown in Table 8 to 10. Three cases are considered according to 25.161 [20]: 1. The lateral and directional trim at the most adverse CG lateral displacement with critical engine inoperative; 2. The longitudinal trim at maximum-power climb and power-off glide with different flap settings; 3. The longitudinal, lateral and directional trim at maximum-power climb with critical engine inoperative. The first and second cases are included in Table 8 and Table 9. These two cases are performed at the 1.3 times reference stall speed V_{SR} and maximum operational speed V_{MO}, which are the minimum and maximum speeds specified in 25.161(b)(c) [20] (note that each flap setting has its own V_{SR} and V_{MO}). The third case is included in Table 10.

Table 8 25.161(b)(c) Trim Certification Constraint Check at $1.3V_{SR}$

Trim Condition	Flap Setting	γ	α	β	δ_e	δ_r	δ_a
Adverse Lateral Condition	Takeoff	0°	9.46°	-3.42°	-5.56°	-9.77°	16.71°
Adverse Lateral Condition	Cruise	0°	4.98°	-1.19°	-4.43°	-3.50°	8.32°
Adverse Lateral Condition	Landing	0°	9.35°	-5.69°	-3.45°	-15.91°	12.99°
Maximum-Thrust Climb	Takeoff	5.74°	9.15°	0°	-3.86°	0°	0°
Maximum-Thrust Climb	Cruise	7.37°	4.84°	0°	-3.50°	0°	0°
Idle-Thrust Glide	Cruise	-3°	5.08°	0°	-4.76°	0°	0°
Idle-Thrust Glide	Landing	-3°	9.45°	0°	-4.22°	0°	0°

Table 9 25.161(b)(c) Trim Certification Constraint Check at V_{MO}

Trim Condition	Flap Setting	γ	α	β	δ_e	δ_r	δ_a
Adverse Lateral Condition	Takeoff	0°	4.03°	-1.85°	-0.79°	-5.35°	11.15°
Adverse Lateral Condition	Cruise	0°	0.91°	-0.54°	-0.40°	-1.59°	3.52°
Adverse Lateral Condition	Landing	0°	3.25°	-3.89°	1.98°	-10.89°	8.44°
Maximum-Thrust Climb	Takeoff	10.60°	3.74°	0°	1.15°	0°	0°
Maximum-Thrust Climb	Cruise	0.17°	0.32°	0°	0.18°	0°	0°
Idle-Thrust Glide	Cruise	-3°	0.43°	0°	0.02°	0°	0°
Idle-Thrust Glide	Landing	-3°	3.26°	0°	1.56°	0°	0°

Table 10 25.161(d) Trim Certification Constraint Check

Trim Condition	Flap Setting	γ	α	β	δ_e	δ_r	δ_a
Critical-Engine-Inoperative Climb	Cruise	3.25°	3.85°	-1.14°	-3.74°	-4.09°	-1.26°

The stability certification analysis results are shown in Figure 17 to 19. The analysis is performed at the corner points on the CG envelope shown in Figure 5. Different colors in each plot represent different combinations of weight and CG. Both longitudinal and lateral eigen-mode analyses are performed at cruise, takeoff, and landing conditions as shown in Figure 17, Figure 18, and Figure 19 respectfully. From these three figures, it can be found that all the dynamic modes are stable since all the eigenvalues are located at the left-half plane of real axis. However, the stability margins of phugoid mode and spiral mode are limited since their roots are close to the real axis. Comparing between configurations, the short-period mode and spiral mode of cruise configuration is more damped than takeoff and landing configurations, and the dutch-roll mode natural frequency of cruise configuration is higher than takeoff and landing configurations.

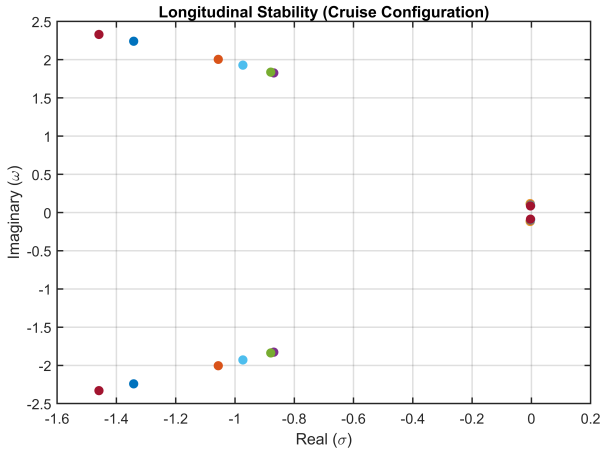

(a) Longitudinal

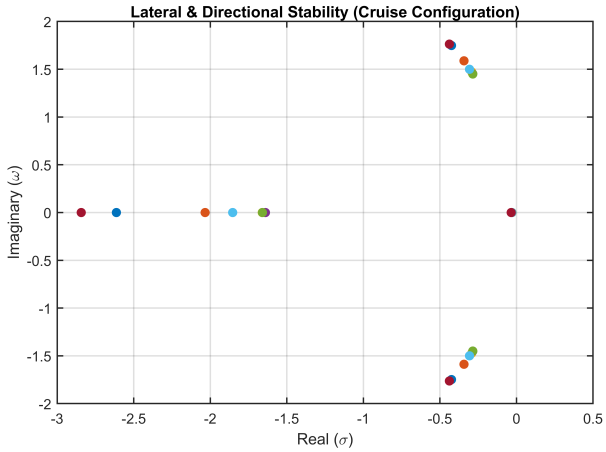

(b) Lateral & Directional

Fig. 17 Cruise Configuration Stability

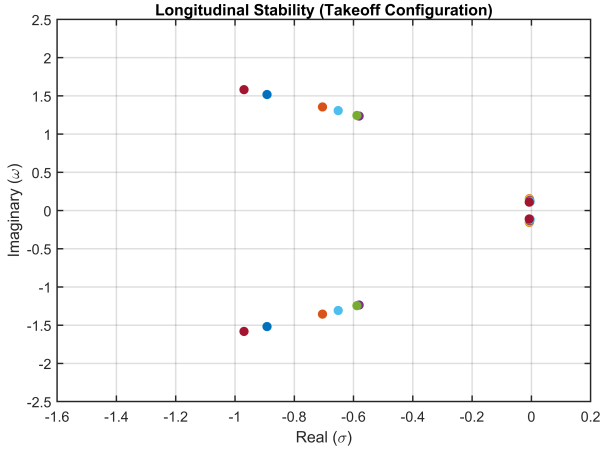

(a) Longitudinal

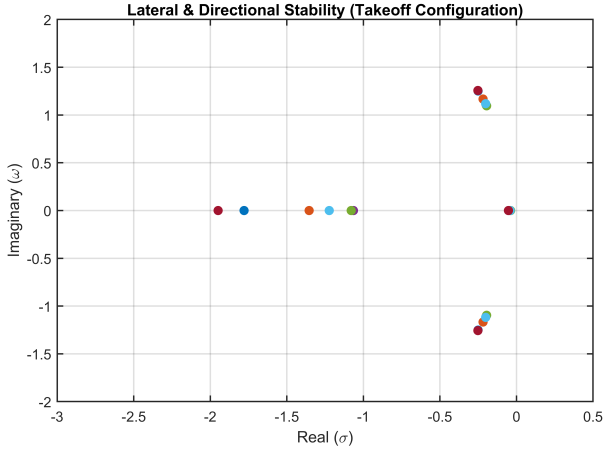

(b) Lateral & Directional

Fig. 18 Takeoff Configuration Stability

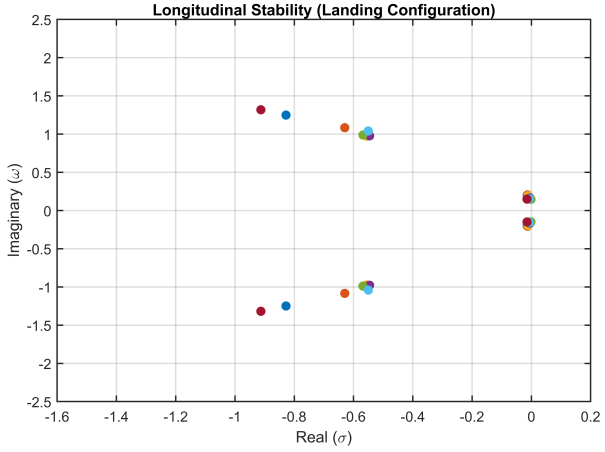

(a) Longitudinal

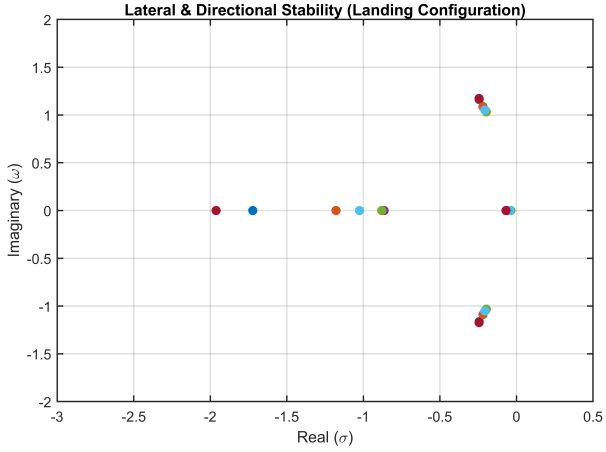

(b) Lateral & Directional

Fig. 19 Landing Configuration Stability

B. Benchmark

The takeoff and landing performance data computed by the certification module are benchmarked against the published data documented in the airport planning [30] and operation manual [31] of Boeing 737-800. The simulation cases for benchmark are conducted at sea-level runway and MTOW/MDLW. The comparison result is shown in Table 11. Because the data of stability and maneuverability of Boeing 737 is not available in public domain, the associated certification analysis cannot be benchmarked.

Table 11 Benchmark Result

Metric	B737-800 Data [30]	Certification Module	Error	FLOPS [22]	Error
Takeoff Field Length (ft)	7780.3	7546.2	-3.01%	10421.6	33.95%
Landing Field Length (ft)	5815.8	5405.5	-7.05%	6550.0	12.62%

According to Table 11, the certification module underestimates the takeoff distance by 3.01% and landing distance by 7.01%. Such error is acceptable in early design stage, especially compared with the analysis result from FLOPS [22] using same input aircraft model. The errors might be caused by the approximation of aerodynamic data, stability & control derivatives, etc. However, if the simulation is performed at higher runway altitudes, comparing Figure 8 and Figure 12 with the aircraft flight manual [30, 31], the error in takeoff and landing field length predictions may become larger. Such difference might be caused by the modeling error in engine deck. In future work, further research effort will be conducted to improve the accuracy of certification module in takeoff and landing simulation at high altitudes.

VIII. Conclusion

This paper presents a method to incorporate certification constraints into aircraft early design stage by developing a certification analysis module. The certification module successfully transforms the flight performance certification regulations from textual documents to quantitative constraint functions, and enables the design scheme to be virtually certified in the early design stage. The development process identified the minimum design knowledge needed to perform the certification check, which also provides guidance to the development of conceptual design analysis tools. With additional sizing and analysis tools being developed and linked to the certification module, it is expected that a new MDAO environment will be formulated and shift forward the design space exploration compared with the tradition design process. The introduction of certification information in early design stage promotes the viability of the design and potentially reduces the cost and time associated with certification process.

The avenues for future work include: 1. Integrate the certification module with disciplinary analyses to formulate a MDAO environment for aircraft design and optimization; 2. Incorporate high-fidelity analysis and uncertainty quantification method with the certification module to establish a certification by analysis environment; 3. Apply the development methodology to other subparts of the FAR-25 to create the certification analysis module for subsystem or component levels constraint check.

Appendix

Table 12 Specifications of Testing Model

Parameter	Value	Unit
Passenger capacity	160	-
Maximum ramp weight	174 870	lb
Design range	3140	nmi
Cruise Mach number	0.85	-
Maximum landing weight	146 300	lb
Sea-level static thrust	$2 \times 27\,297$	lb
Wing planform area	1408.5	ft^2
Wingspan	113.15	ft
Mean aerodynamic chord	11.85	ft
Wing aspect ratio	9.74	-
Wing taper ratio	0.28	-
Wing 1/4-chord sweep	25.72	deg
Wing dihedral	5.69	deg
Aileron chord ratio	0.15	-
Aileron locations (fraction of semi-span)	0.62; 0.83	-
Fuselage total length	124.75	ft
Maximum fuselage width	12.33	ft
Maximum fuselage height	13.17	ft
Horizontal tail planform area	359.22	ft^2
Horizontal tail aspect ratio	6.27	-
Horizontal tail taper ratio	0.20	-
Horizontal tail 1/4-chord sweep	29.91	deg
Elevator chord ratio	0.25	-
Elevator locations (fraction of semi-span)	0.06; 1.00	-
Vertical tail planform area	277.76	ft^2
Vertical tail aspect ratio	1.92	-
Vertical tail taper ratio	0.28	-
Vertical tail 1/4-chord sweep	35.00	deg
Rudder chord ratio	0.25	-
Rudder locations (fraction of semi-span)	0.05; 0.98	-

References

[1] "Certifying Boeing's Airplanes," , 2013. URL http://787updates.newairplane.com/Certification-Process.

[2] Perret, B., "ARJ21 Delayed Again, Due To Enter Service April-May 2015," , Jan. 2014. URL http://aviationweek.com/commercial-aviation/arj21-delayed-again-due-enter-service-april-may-2015.

[3] Perrett, B., "Mitsubishi MRJ Delivery Delayed Until Mid-2020," , Jan. 2017. URL http://aviationweek.com/commercial-aviation/mitsubishi-mrj-delivery-delayed-until-mid-2020.

[4] Mangelsdorf, M., "Environmentally Responsible Aviation N+2 Advanced Vehicle Concepts NRA Status," , Jun. 2011. URL https://ntrs.nasa.gov/archive/nasa/casi.ntrs.nasa.gov/20110015351.pdf.

[5] Ratliff, C., and Marquart, E., "An assessment of a potential test technique - Virtual Flight Testing (VFT)," *Flight Simulation Technologies Conference*, American Institute of Aeronautics and Astronautics, 1995. doi:10.2514/6.1995-3415.

[6] Gebert, G., Kelly, J., Lopez, J., and Evers, J., "Wind tunnel based virtual flight testing," *38th Aerospace Sciences Meeting and Exhibit*, American Institute of Aeronautics and Astronautics, 2000. doi:10.2514/6.2000-829.

[7] Burdun, I., DeLaurentis, D., and Mavris, D., "Modeling and simulation of airworthiness requirements for an HSCT prototype in early design," *7th AIAA/USAF/NASA/ISSMO Symposium on Multidisciplinary Analysis and Optimization*, American Institute of Aeronautics and Astronautics, 1998. doi:10.2514/6.1998-4936.

[8] Scharl, J., Mavris, D., and Burdun, I., "Use of flight simulation in early design - Formulation and application of the virtual testing and evaluation methodology," *2000 World Aviation Conference*, American Institute of Aeronautics and Astronautics, 2000. doi:10.2514/6.2000-5590.

[9] "Flight Path 2050 Europe's vision for aviation: maintaining global leadership and serving society's needs," Tech. rep., European Commission, Jun. 2011. doi:10.2777/50266.

[10] Solar, D., "Aircraft Certification and Simulation — Current Practice, Future Outlooks and Challenges," , Sep. 2014. URL http://airtn.eu/wp-content/uploads/2_airtn-nextgen-certification-and-simulation.pdf.

[11] Kroll, N., Abu-Zurayk, M., Dimitrov, D., Franz, T., Führer, T., Gerhold, T., Görtz, S., Heinrich, R., Ilic, C., Jepsen, J., Jägersküpper, J., Kruse, M., Krumbein, A., Langer, S., Liu, D., Liepelt, R., Reimer, L., Ritter, M., Schwöppe, A., Scherer, J., Spiering, F., Thormann, R., Togiti, V., Vollmer, D., and Wendisch, J.-H., "DLR project Digital-X: towards virtual aircraft design and flight testing based on high-fidelity methods," *CEAS Aeronautical Journal*, Vol. 7, No. 1, 2015, pp. 3–27. doi:10.1007/s13272-015-0179-7.

[12] Schmollgruber, P., Bedouet, J., Bartoli, N., and Gourinat, Y., "Development of a Certification Module tailored to Aircraft Multidisciplinary Design Optimization," *Challenges in European Aerospace, 5th CEAS Air & Space Conference*, 2015. URL http://aerospace-europe.eu/media/books/CEAS2015_150.pdf.

[13] Schmollgruber, P., Bartoli, N., and Gourinat, Y., "Virtual flight testing in an aircraft sizing and optimization process," *15th AIAA Aviation Technology, Integration, and Operations Conference*, American Institute of Aeronautics and Astronautics, 2015. doi:10.2514/6.2015-2546.

[14] Schmollgruber, P., Bartoli, N., Bedouet, J., Defoort, S., Gourinat, Y., Benard, E., Lafage, R., and Sgueglia, A., "Use of a Certification Constraints Module for Aircraft Design Activities," *17th AIAA Aviation Technology, Integration, and Operations Conference*, American Institute of Aeronautics and Astronautics, 2017. doi:10.2514/6.2017-3762.

[15] Goron, G., Duca, R., Sarojini, D., Shah, S., Chakraborty, I., Briceno, S. I., and Mavris, D. N., "A Simulation-Based Framework for Structural Loads Assessment during Dynamic Maneuvers," *17th AIAA Aviation Technology, Integration, and Operations Conference*, American Institute of Aeronautics and Astronautics, 2017. doi:10.2514/6.2017-3767.

[16] Wendorff, A. D., Alonso, J. J., and Bieniawski, S. R., "A Multi-Fidelity Approach to Quantification of Uncertainty in Stability and Control Databases for use in Stochastic Aircraft Simulations," *16th AIAA/ISSMO Multidisciplinary Analysis and Optimization Conference*, American Institute of Aeronautics and Astronautics, 2015. doi:10.2514/6.2015-3439.

[17] Casalino, D., Noelting, S., Fares, E., de Ven, T. V., Perot, F., and Bres, G., "Towards Numerical Aircraft Noise Certification: Analysis of a Full-Scale Landing Gear in Fly-Over Configuration," *18th AIAA/CEAS Aeroacoustics Conference (33rd AIAA Aeroacoustics Conference)*, American Institute of Aeronautics and Astronautics, 2012. doi:10.2514/6.2012-2235.

[18] Abdi, F., Li, Q., Zhu, X., Zhu, G., Chen, Y., Baid, H. K., and Housner, J., "Wheels Up Landing Certification By Analysis of Regional Jet Aircraft," *2018 AIAA Aerospace Sciences Meeting*, American Institute of Aeronautics and Astronautics, 2018. doi:10.2514/6.2018-0763.

[19] Abdi, F., Song, C., Kong, L., Li, N., Wu, Z., Baid, H. K., and Huang, D., "Bird Strike Certification by Analysis of ARJ21 Multi-Functional Vertical Stabilizer," *2018 AIAA Aerospace Sciences Meeting*, American Institute of Aeronautics and Astronautics, 2018. doi:10.2514/6.2018-0766.

[20] *Code of Federal Regulations, Title 14, Federal Aviation Regulations, Part 25 - Airworthiness Standards: Transport Category Airplanes*, Federal Aviation Administration, 2019. URL https://www.ecfr.gov/cgi-bin/text-idx?SID=01562311885680c5924c66bdbc66b2c&mc=true&node=pt14.1.25&rgn=div5.

[21] *Advisory Circular AC 25-7D Flight Test Guide for Certification of Transport Category Airplanes*, Federal Aviation Administration, May 2018. URL https://www.faa.gov/documentLibrary/media/Advisory_Circular/AC_25-7D.pdf.

[22] McCullers, L., *Flight Optimization System, Release 8.11, User's Guide*, NASA Langley Research Center, Hampton, VA 23681-0001, Oct. 2009.

[23] Wells, D. P., Horvath, B. L., and McCullers, L. A., "The Flight Optimization System Weights Estimation Method," Tech. rep., 2017.

[24] Roskam, D. J., *Airplane Design Part VI : Preliminary Calculation of Aerodynamic Thrust and Power Characteristics*, Design, Analysis and Research Corporation (DARcorporation), 2017.

[25] Drela, M., and Youngren, H., *AVL 3.36 User Primer*, MIT, Feb. 2017.

[26] Etkin, B., and Engineering, *Dynamics of Atmospheric Flight (Dover Books on Aeronautical Engineering)*, Dover Publications, 2005.

[27] LAMBREGTS, A., "Vertical flight path and speed control autopilot design using total energy principles," *Guidance and Control Conference*, American Institute of Aeronautics and Astronautics, 1983. doi:10.2514/6.1983-2239.

[28] Chakraborty, I., Lozano, B., and Mavris, D. N., "Pilot-Friendliness Considerations for Personal Air Vehicle Flight Control Systems," *15th AIAA Aviation Technology, Integration, and Operations Conference*, American Institute of Aeronautics and Astronautics, 2015. doi:10.2514/6.2015-2852.

[29] Chakraborty, I., "Subsystem architecture sizing and analysis for aircraft conceptual design," Ph.D. thesis, Georgia Institute of Technology, 2015. URL https://smartech.gatech.edu/handle/1853/54427.

[30] *737 Airplane Characteristics for Airport Planning*, Boeing Commercial Airplanes, Sep. 2013. URL http://www.boeing.com/assets/pdf/commercial/airports/acaps/737.pdf.

[31] *737-600/-700/-800/-900 Operations Manual*, The Boeing Company, 10^{th} ed., Sep. 2002. URL http://www.737flightsimulator.co.uk/737info/B737OM.pdf.